Acupuncture and Herbal Medicine

Discovery of soluble epoxide hydrolase inhibitors based on the skeleton of piperine: synthesis, properties, molecular dynamics simulation, and their potentials in acute lung injury

Juan Zhang[1,2], Xue-Tao Yang[3], Min Zhang[1], Qi-Meng Zhu[1], Da-Hong Yao[3,*], Xiao-Chi Ma[4,*], Bruce D. Hammock[2,*], Cheng-Peng Sun[1,*]

[1]School of Chinese Materia Medica, School of Medical Technology, Tianjin Key Laboratory of Therapeutic Substance of Traditional Chinese Medicine, Tianjin University of Traditional Chinese Medicine, Tianjin, China; [2]Department of Entomology and Nematology, UC Davis Comprehensive Cancer Center, University of California, Davis, CA, USA; [3]School of Pharmaceutical Sciences, Shenzhen Technology University, Shenzhen, China; [4]Second Affiliated Hospital, Dalian Medical University, Dalian, China

Abstract

Objective: Soluble epoxide hydrolase (sEH) emerges as a target of interest for inflammatory diseases. Piperine is a natural amide alkaloid from *Piper nigrum* and displays an inhibitory effect toward sEH, its chemical structural transformation was carried out in order to obtain a library of sEH inhibitors based on its skeleton.

Methods: Structural transformation of piperine was carried out by chemical methods, and piperine derivatives were assayed for their sEH potentials. A mouse acute lung injury model was constructed by lipopolysaccharide (LPS). Hematoxylin and eosin (H&E) staining, immunofluorescence staining, Western Blot, and enzyme-linked immunosorbent assay were used for investigating the protective potential of sEH inhibitor **11h**.

Results: Piperine derivatives **11e**, **11h**, **11j**, and **11o** showed inhibitory potentials toward sEH with values of half maximal inhibitory concentration (IC_{50}) from 20 to 70 nM. Compound **11h** attenuated the pathological course of LPS-mediated acute lung injury (ALI) *in vivo*. Furthermore, levels of cytokines tumor necrosis factor alpha (TNF-α), interleukin 6 (IL-6), myeloperoxidase (MPO), and lactate dehydrogenase (LDH) were decreased after administration of **11h**. The LPS-mediated inflammation and redox unbalance, including expressions of cyclooxygenase-2 (COX-2), heme oxygenase-1 (HO-1), intercellular cell adhesion molecule-1 (ICAM-1), vascular cell adhesion molecule-1 (VCAM-1), p-p65/p65, glutamate-cysteine ligase modifier subunit (GCLM), and nuclear factor erythroid-2-related factor 2 (Nrf2), were ameliorated through nuclear factor kappa B (NF-κB) and Nrf2 pathways *via* enhancing levels of epoxyeicosatrienoic acids (EETs) in LPS-exposed ALI mice after compound **11h** treatment. Molecular docking demonstrated that the aromatic unsaturated group of **11h** occupied a hydrophobic pocket and its urea group formed three hydrogen bonds with Asp333, Tyr381, and Tyr465, which stabilized the active conformation of the ligand.

Conclusions: These findings demonstrated that compound **11h** may serve as a lead compound for developing sEH inhibitors and treating inflammation related to diseases, such as ALI.

Keywords: Inflammation, Piperine, Soluble epoxide hydrolase, Structure–activity relationship

Graphical abstract: http://links.lww.com/AHM/A153.

Introduction

Arachidonic acid (AA) is a C_{20} fatty acid with four *cis*-form olefinic bonds and belongs to the family of the ω-6 polyunsaturated fatty acids (PUFAs)[1]. AA is mainly located in the phospholipid layer of the cell membrane or stored in the liposome of immune cells[2]. At the cellular level, AA is released from phospholipids under the action of three main phospholipases A2 (PLA2), C (PLC), and D (PLD)[3–5], and further metabolized *via* three main pathways: cytochrome p450 (Cyp450), lipoxygenase (LOX), and cyclooxygenase (COX)[6]. For example, Cyp2c and 2j can readily epoxidize the double

Juan Zhang and Xue-Tao Yang contributed equally to this work.

**Corresponding authors. Da-Hong Yao, E-mail: yaodahong@sztu.edu.cn; Xiao-Chi Ma, E-mail: maxc1978@163.com; Bruce D. Hammock, E-mail: bdhammock@ucdavis.edu; Cheng-Peng Sun, E-mail: suncp146@163.com.*

Received 17 January 2024 / Accepted 12 February 2025

***How to cite this article:** Zhang J, Yang XT, Zhang M, Zhu QM, Yao DH, Ma XC, Hammock BD, Sun CP. Discovery of soluble epoxide hydrolase inhibitors based on the skeleton of piperine: synthesis, properties, molecular dynamics simulation, and their potentials in acute lung injury. Acupunct Herb Med 2025;5(2):193–204. DOI: 10.1097/HM9.0000000000000148*

bond of AA to form four kinds of epoxyeicosatrienoic acids (EETs) (eg, 5,6-, 8,9-, 11,12-, and 14,15-EETs) that possess remarkable physiological effects[6], such as vasodilation and the inhibition of Na^+ transportation[7–9]. However, soluble epoxide hydrolase (sEH) is in charge of EETs and other epoxy fatty acids (EpFAs) hydrolysis, yielding their corresponding diols (eg, dihydroxyeicosatrienoic acids [DHETs] and other dihydroxy fatty acids), which will lead to the inactivation of formers[6,10–12]. Therefore, sEH attracts the attention of scientists.

sEH is a domain-swapped homodimer with 555 amino acids comprising of an N-terminal phosphatase (amino acids from 1 to 218) and C-terminal hydrolase domains (amino acids from 235 to 555)[7,13]. Compared with its N-terminal function, its C-terminal function has been investigated in depth because of the hydrolyzation of bioactive metabolites EETs and other EpFAs[6,14]. Similar to other hydrolases, the hydrolase function of sEH depends on Asp333, Tyr381, Tyr465, Asp495, and His523 in charge of the formation of an oxyanion hole that stabilizes the intermediate product during the epoxide hydrolysis reaction[15–17]. A line of studies have illustrated that stabilizing levels of EETs by suppressing sEH improves peripheral inflammation and neuroinflammatory diseases[6,10,14–22]. For example, kurarinone, a natural sEH inhibitor from *Sophora flavescens*, promotes the increase of levels of EETs to inactivate the nuclear factor kappa B (NF-κB) pathway, allowing the remission of 1-methyl-4-phenyl-1,2,3,6-tetrahydropyridine (MPTP)-mediated neuroinflammation in Parkinson disease[15]. Moreover, wedelolactone, a furan-type coumarin, targets sEH to attenuate inflammation and unbalance of redox system in acute lung injury (ALI)[16]. Meanwhile, sEH genetic deletion alleviates PD and acute kidney injury in the animal model[6,15–16,18]. Therefore, more and more scientists paid attention to the discovery of sEH inhibitors.

So far, sEH inhibitors have been classified into two groups, natural products and chemical synthesis[6], while the latter could further be divided into urea (eg, TPPU, AUDA, *t*-AUCB, AR-9281, and EC-5026) and amide (eg, MTTP and GSK2256294) sEH inhibitors[6,23]. Among them, AR-9281, GSK2256294, and EC-5026 have entered human clinical trials for treating hypertension, and neuropathic and inflammatory pain, respectively[24–25]. Recently, the screening of sEH inhibitors from natural products resulted in the discovery of alisol B, kuraronine, wedelolactone, piperlonguminine, britanicafanin B, 3*β*-hydroxy-25-anhydro-alisol F, capsaicin, dihydrocapsainin, and futoamide[6,8,15–18,26]. Because of the role of sEH in diseases referred to inflammation, a series of sEH inhibitors was afforded according to the skeleton of piperine, a natural amide alkaloid from *Piper nigrum*, and their inhibitory potentials were evaluated, which revealed nanomolar potentials of compounds **11e**, **11h**, **11j**, and **11o**. The *in vivo* experimental result demonstrated that inhibition of sEH by compound **11h** could alleviate lipopolysaccharide (LPS)-mediated ALI in the mouse model by doubly suppressing inflammation and oxidative stress, which showed that compound **11h** is a candidate in the treatment of ALI.

Materials and methods

General experimental procedures

^1H and ^{13}C nuclear magnetic resonance (NMR) spectra were recorded by a Bruker NMR spectrometer (Bruker, Karlsruhe, Germany), and the solvents $CDCl_3$ and dimethylsulfoxide (DMSO)-d_6 were considered as the reference (δ_H 7.27 and 2.50; δ_C 77.2 and 39.5). High resolution electrospray ionization mass spectroscopy (HR-ESI-MS) data were recorded on an AB SCIEX X500R Q-TOF mass spectrometer (Scientific Export [SCIEX], USA).

Synthesis of compounds 11a–t

Intermediate **10** (100 mg, 0.35 mmol) was dissolved in CH_2Cl_2 and reacted with isocyanate derivatives (0.35 mmol) and DIPEA (115.0 μL, 0.7 mmol). After five hours, H_2O was added to this reaction system to afford CH_2Cl_2 extract. After removing the solvent, residues were separated through a silica gel column and eluted with CH_2Cl_2/MeOH (from 95:5 to 10:1) to obtain compounds **11a** to **t**. Their detailed spectral data are listed in Supplementary Material, http://links.lww.com/AHM/A154.

Molecular docking

The molecular docking of **11h** within sEH (PDB code 1ZD4) was performed by Discovery Studio 3.5[27]. The active docking pocket is determined based on the cavity of the reference ligand (13.0 Å sphere). The Charmm forcefield was chosen as the docking forcefield. The adding hydrogen atoms and energy minimization were applied with **11h**.

sEH inhibitory assay

All the synthesized compounds were assayed for inhibitory effects toward sEH based on the method of probe substrate PHOME[14–16,18]. All the compounds were preincubated with sEH (0.1 ng/mL, Tris-HCl buffer) for 3 minutes, and then added substrate PHOME (10 μM). After 20 minutes, the reaction was terminated with acetonitrile (100 μL), and the signal (λem 330 nm and 7ex 465 nm) was detected by a microplate reader.

Animal and treatment

C57BL/6 mice (male, 8 weeks old, the Experimental Animal Center of Dalian Medical University) were classified into the control, compound **11h** (5 mg/kg), LPS (5 mg/kg), and LPS plus compound **11h** (2.5 or 5 mg/kg) groups, randomly. Mice in five different groups were administrated with the vehicle or compound **11h** (2.5 or 5 mg/kg) for 7 days through intragastric administration and further treated with the vehicle or LPS (5 mg/kg) through intratracheal instillation after the final intragastric administration of the vehicle or compound **11h**[28–29]. After 24 h, mice were sacrificed, and lung samples were collected for analysis levels of interleukin 6 (IL-6), tumor

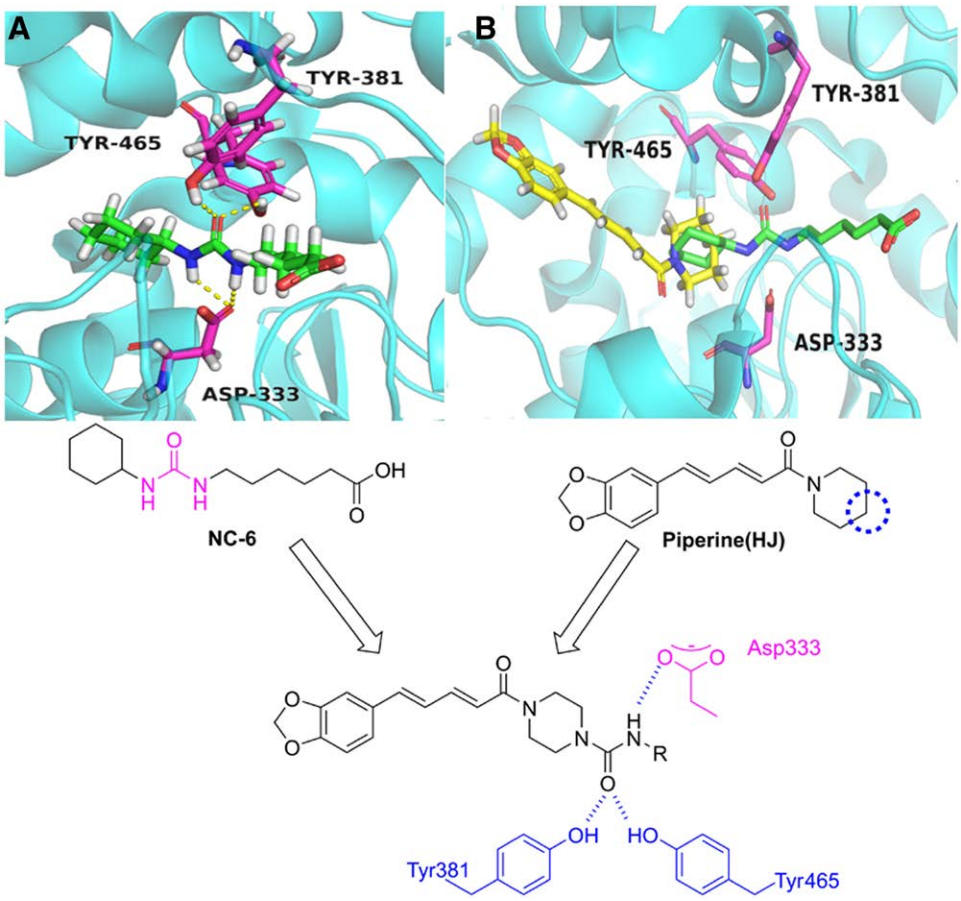

Figure 1. The optimization of piperine as A inhibitors. (A) The hydrogen bond interaction of TPPU with sEH. (B) The overlapped plot of TPPU (green) and piperine (yellow) with sEH. sEH: Soluble epoxide hydrolase.

necrosis factor alpha (TNF-α), myeloperoxidase (MPO), and lactate dehydrogenase (LDH).

Distribution of compound 11h in tissues

Mice were intragastric administrated with compound **11h** (10 mg/kg). After 20 min, mice were anesthetized, and all the tissues were collected. Samples suspended by H_2O were extracted with ethyl acetate (EtOAc), and the organic layer were analyzed by an LC-MS/MS system.

Immunohistochemistry and immunofluorescence staining

Lung samples were soaked in the tissue fixation solution, embedded with paraffin, and cut into sections (4 μm). The sections were stained with the H&E kit. For immunofluorescence staining, sections were dewaxed by xylene and different concentrations of ethanol, blocked with 10% goat serum, and treated with primary antibodies CD68 and Gr-1 and fluorescent secondary antibodies after the antigen retrieval, successively. Finally, sections were recorded on a Leica DM4B microscope (Leica, Germany)[28–29].

Real time-quantitative polymerase chain reaction (qPCR)

Samples were lysed with a TRIzol reagent, followed by the reverse transcription to obtain cDNA. Real-time qPCR using TransStart Tip Green qPCR SuperMix was conducted on a qPCR System[16,30–31].

Western blot

Lungs were lysed with the lysis buffer (1% cocktail and 1% phenylmethanesulfonyl fluoride [PMSF]), added in loading buffer, and boiled at 95°C for 10 minutes to afford total protein samples. Proteins were subjected to 10% to 12% SDS-PAGE and transferred to PVDF membranes. The blocked membranes were incubated with primary antibodies, washed with TBST, incubated with the secondary antibody, and finally analyzed by the Tanon 5200-ECL detection system.

Results and discussion

Structure optimization of piperine as sEH inhibitors

Piperine displays a sEH inhibitory activity (half maximal inhibitory concentration [IC_{50}] = 35.1 μM), making it a promising lead to optimize for novel potent sEH inhibitors. The crystal structure of sEH/NC-6 (PDB code 1ZD4) suggested that the urea group of ligand (NC-6) was indispensable for the inhibitory potency against sEH by initiating four conserve hydrogen interactions with residues Asp333, Tyr381, and Tyr465. Next, we conducted molecular docking of piperine and sEH. The results revealed that the unsaturated aromatic group of piperine occupied a hydrophobic pocket, while the piperidine group located a similar site with cyclohexyl of NC-6. We envisaged the introduction of a urea moiety into the piperidine ring to form a similar hydrogen bond network to improve affinity (Figure 1).

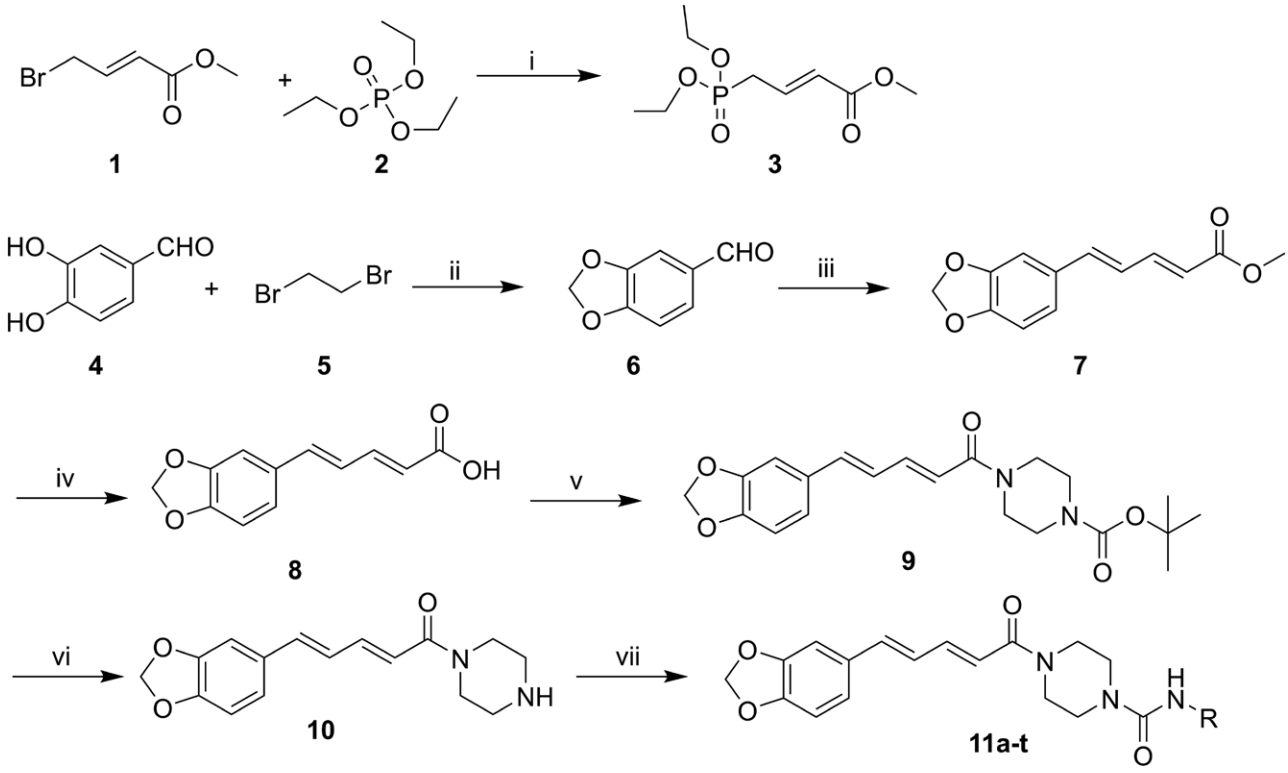

Figure 2. Synthesis of compounds **11a-t**. Reagents and conditions: (i) 130°C, 4 h; (ii) K_2CO_3, DMF, 90°C, 12 h; (iii) LiOH, THF, reflux, 4 h; (iv) 1N NaOH (50% methanol); (v) HBTU, DIPEA, tert-butyl 1-piperazinecarboxylate, DMF, r.t.; (vi) CH_2Cl_2/TEA (1:1), r.t.; (vii) isocyanate derivatives, CH_2Cl_2, DIPEA, r.t. DIPEA: N,N-diisopropylethylamine; DMF: Dimethyl formamide; HBTU: O-benzotriazol-1-yl-N,N,N',N'-tetramethyluronium hexafluorophosphate; TEA: Triethylamine.

Chemistry

The preparation of **11a** to t is shown in Figure 2. The unsaturated aromatic scaffold (intermediate **7**) was prepared by a modified Wittig reaction of intermediate **6** with **3**. The product was further hydrolyzed under LiOH condition, condensed with tert-butyl 1-piperazine carboxylate, deprotected, and interacted with isocyanate derivatives to produce **11a** to **t**.

Analysis of the structure–activity relationship

To afford sEH inhibitors based on the structure of piperine (IC_{50} = 35.1 μM, Table 1), we first replaced the piperidine group of piperine with piperazine to yield **10**, which resulted in a complete loss in activity against sEH. Next, a urea group was induced to the 4-site of piperazine with *p*-methyl phenyl to produce **11a** (IC_{50} = 0.86 μM), **11a** was about 40 times more potent than piperine in inhibitory potency against sEH. An additional methyl was incorporated into 2-site of phenyl to obtain **11b** presenting a significant decrease in inhibitory activity against sEH (IC_{50} = 6.58 μM). We further modified **11b** to obtain **11c** to **11e** by inducing some electron substituent. The results displayed that **11e** with an isopropyl substituent displayed the most potent activity (IC_{50} = 0.02 μM). Encouraged by the good inhibitory potency of **11e**, **11f** to **11i** were synthesized with chlorine substitutions in different positions. The para-substituted compounds (**11f** and **11h**) showed better inhibitory activities (IC_{50}, 0.29 and 0.04 μM). Similarly, **11j** with a Br in para-substituted displayed a potent inhibitory activity (IC_{50} = 0.07 μM). In addition, we further incorporated some potent electron-absorbing groups, such as fluorine, trifluoromethyl, and cyano groups. The fluorine substitutions (**11k–11n**) led to a significant decrease in activity, and the trifluoromethyl in para- and inter-substituted (**11o** and **11p**) led to an improvement in inhibitory activities (IC_{50}, 0.02 and 0.18 μM). The cyano substitution (**11r**) showed a slight decrease in its inhibitory activity. Collectively, the urea group plays a critical role in maintaining inhibitory effects toward sEH, and certain sizes of both electron-withdrawing and electron-donating groups are tolerated to improve the inhibitory activity.

Molecular docking and molecular dynamic simulation

We conducted a molecular docking to clarify the binding mode of **11h** with sEH by Discovery Studio 3.5. The results revealed that the aromatic unsaturated group of **11h** occupied a hydrophobic pocket and the urea moiety formed three hydrogen interactions with Asp333, Tyr381, and Tyr465, which stabilized the active conformation of the ligand (Figure 3A–D). The phenyl occupied an additional pocket initiating a key Pi–Pi stacked interaction with amino acid residue His523. Furthermore, the 3- and 4-site chlorine electron substituents formed two pairs of Halogen interactions with amino acid residues Leu406, Met418, Val497, and Trp524 (Figure 3D). Collectively, **11h** is a new potent sEH inhibitor. In 100 ns MD simulation, root mean square deviation (RMSD) of sEH around 5 Å of **11h** fluctuated between 0.6 and 1.7, indicating that its binding to sEH presented fairly stable active profiles (Figure 3E). Figure 3F demonstrates that **11h** showed the strongest binding affinity with sEH, supporting its inhibitory potential (Table 2 and Figure 3F). In addition, the residue's energy decomposition indicated

Table 1

IC_{50} values of piperine and its derivatives toward sEH

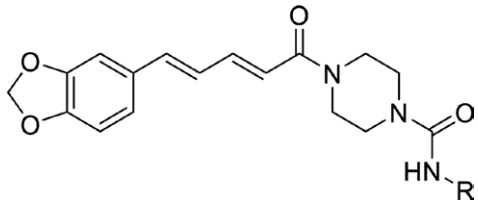

Compound	R	Inhibitory activity (IC_{50} ± SD, μM)
Piperine	-	35.13 ± 1.22
9	-	61.25 ± 2.38
10	-	>100
11a	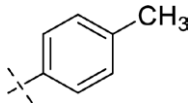	0.86 ± 0.15
11b	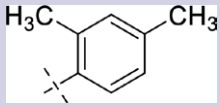	6.58 ± 0.14
11c	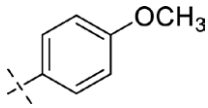	1.53 ± 0.16
11d	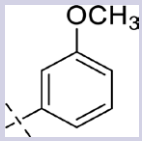	4.24 ± 0.61
11e	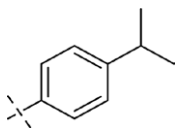	0.02 ± 0.01
11f	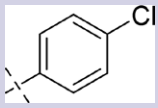	0.29 ± 0.02
11g	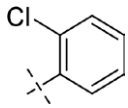	8.98 ± 0.09
11h	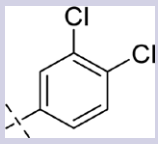	0.04 ± 0.01
11i	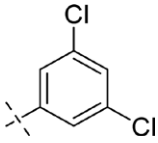	2.28 ± 1.32
11j	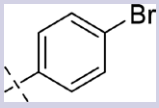	0.07 ± 0.01
11k	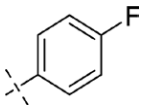	7.62 ± 0.81

(*Continued*)

Table 1
(Continued)

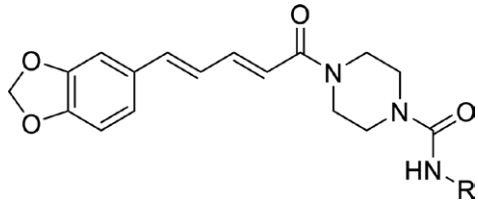

Compound	R	Inhibitory activity (IC_{50} ± SD, μM)
11l	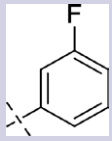	3.91 ± 1.10
11m	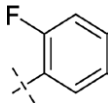	8.83 ± 1.29
11n	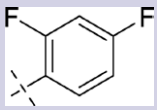	4.02 ± 1.06
11o	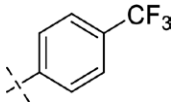	0.02 ± 0.01
11p	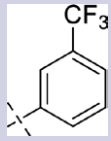	0.18 ± 0.04
11q	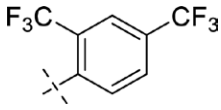	3.74 ± 0.01
11r	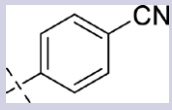	0.31 ± 0.06
11s	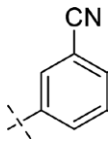	6.39 ± 0.78
11t	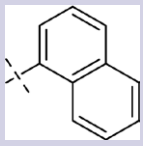	8.48 ± 1.70
TPPU	-	0.01 ± 0.01

IC_{50}: Half maximal inhibitory concentration; sEH: Soluble epoxide hydrolase.

that nonpolar energy contribution from residues Phe265, Trp334, Met337, Ile361, Pro369, Val497, and Leu498 played a key role in the binding of **11h** and sEH.

Compound 11h attenuated the pathological course of LPS-mediated ALI

Compounds **11e**, **11h**, and **11o** showed potent inhibitory effects toward sEH with IC_{50} values in the range of 20 to 40 nM, which encouraged us to investigate their potential for diseases. First, we determined the tissue distribution of compound **11h** after 20 min of its oral administration and found that it was mainly distributed in lung (187.3 ng/g) and kidney (172.6 ng/g, Figure 4A). A series of studies have demonstrated that sEH genetic deletion could attenuate inflammation-mediated lung injury, such as ALI[16,32–33], and its inhibitors TPPU and AUDA alleviated pulmonary

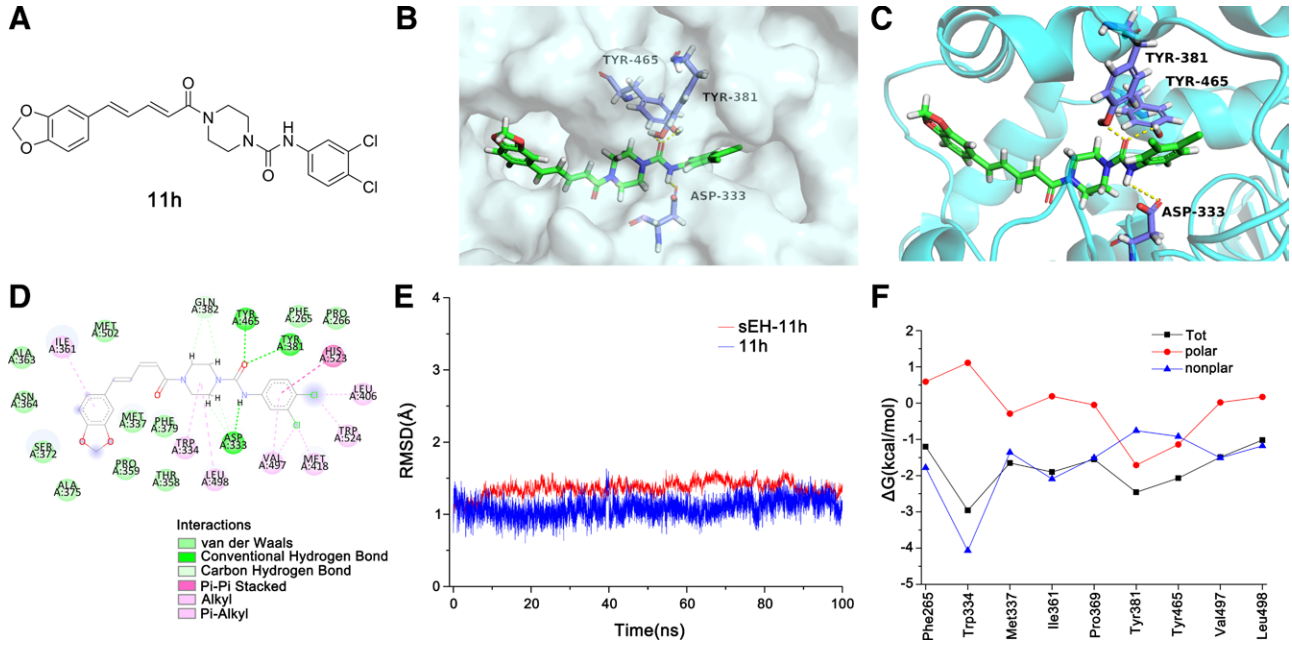

Figure 3. Molecular docking of **11h** and sEH. (A) Structure of **11h**; (B) surface view of **11h**–sEH complex; (C) 3D view of **11h**–sEH; (D) Detailed interactions of **11h**–sEH; (E) RMSD of sEH with or without **11h**; (F) Residues energy decomposition of **11h** with sEH. RMSD: Root mean square deviation; sEH: Soluble epoxide hydrolase.

Table 2

The binding free energies were calculated by MM-GBSA method (kcal/mol)

Compound	ΔE_{ele}	ΔE_{vdw}	$\Delta G_{sol\text{-}np}$	$\Delta G_{sol\text{-}ele}$	ΔG_{polar}*	$\Delta G_{nonpolar}$†	ΔH_{bind}	TΔS	ΔG_{bind}
11h	–44.31	–58.26	–7.90	55.18	10.87	–66.16	–55.29	–25.06	–30.23

MM-GBSA: Molecular mechanics poisson-boltzmann surface area.
*$\Delta G_{polar} = \Delta E_{ele} + \Delta E_{vdw}$.
†$\Delta G_{nonpolar} = \Delta G_{vdw} + \Delta G_{sol\text{-}np}$.

inflammation as well[32–34]. Because of the most distribution of compound **11h** in lung and the effect of sEH in pulmonary diseases, we tried to investigate its pulmonary protective effect of compound **11h** in LPS-mediated lung injury (Figure 4B). LPS exposure resulted in pulmonary edema and collapse of alveoli, whereas compound **11h** (2.5 and 5 mg/kg) concentration-dependently attenuated the abovementioned changes (Figure 4C and E). Accumulated evidence has illustrated that macrophages are activated by LPS, leading to the recruitment of neutrophils through inflammatory cytokines IL-6 in the course of ALI[16,35–36]. CD68 and Gr-1, markers of macrophages and neutrophils[28–29], respectively, were used to detect the effects of compound **11h** on macrophages and neutrophils. Figure 4D shows that compound **11h** inactivated macrophages and the recruitment of neutrophils induced by macrophage activation in LPS-exposed mice (Figure 4F and G). Cytokines TNF-α, IL-6, MPO, and LDH are the direct indexes to reflect the degree of pulmonary injury, and we found that compound **11h** could decrease their levels in LPS challenge mice (Figure 5A and B). These results demonstrated the remission effect of compound **11h** toward the pathological changes of ALI.

Compound 11h enhanced levels of EETs, leading to the inhibition of the NF-κB activation

A series of evidence revealed that inhibition of the sEH activity could stabilize levels of its substrates (eg, 11,12-EET), leading to the anti-inflammation through the classical inflammatory pathway—NF-κB[6,14–16,18,37–39]. For example, wedelolactone bound to the catalytic cavity of sEH through Phe362 and Gln384 to inactive sEH activity, allowing its anti-ALI effect through the NF-κB pathway[16]. Similarly, suppressing sEH by kurarinone displayed the anti-neuroinflammatory potential in PD as well[15]. Therefore, we detected the effects of compound **11h** on EETs by LC-MS/MS and the NF-κB pathway. As described in Figure 6, LPS exposure reduced levels of sEH substrates, including 8,9-, 11,12-, and 14,15-EET, while increasing their levels after inhibition of sEH by compound **11h** treatment. Administration of compound **11h** suppressed the increase of inflammatory genes *IL-6*, *TNF-α*, *intercellular cell adhesion molecule-1* (*ICAM-1*), and *vascular cell adhesion molecule-1* (*VCAM-1*) in the lung of LPS-mediated ALI mice (Figure 7A). The NF-κB pathway was inactivated in LPS-exposed mice after administration of compound **11h** because of the decrease of levels of phosphorylated p65 and its downstream

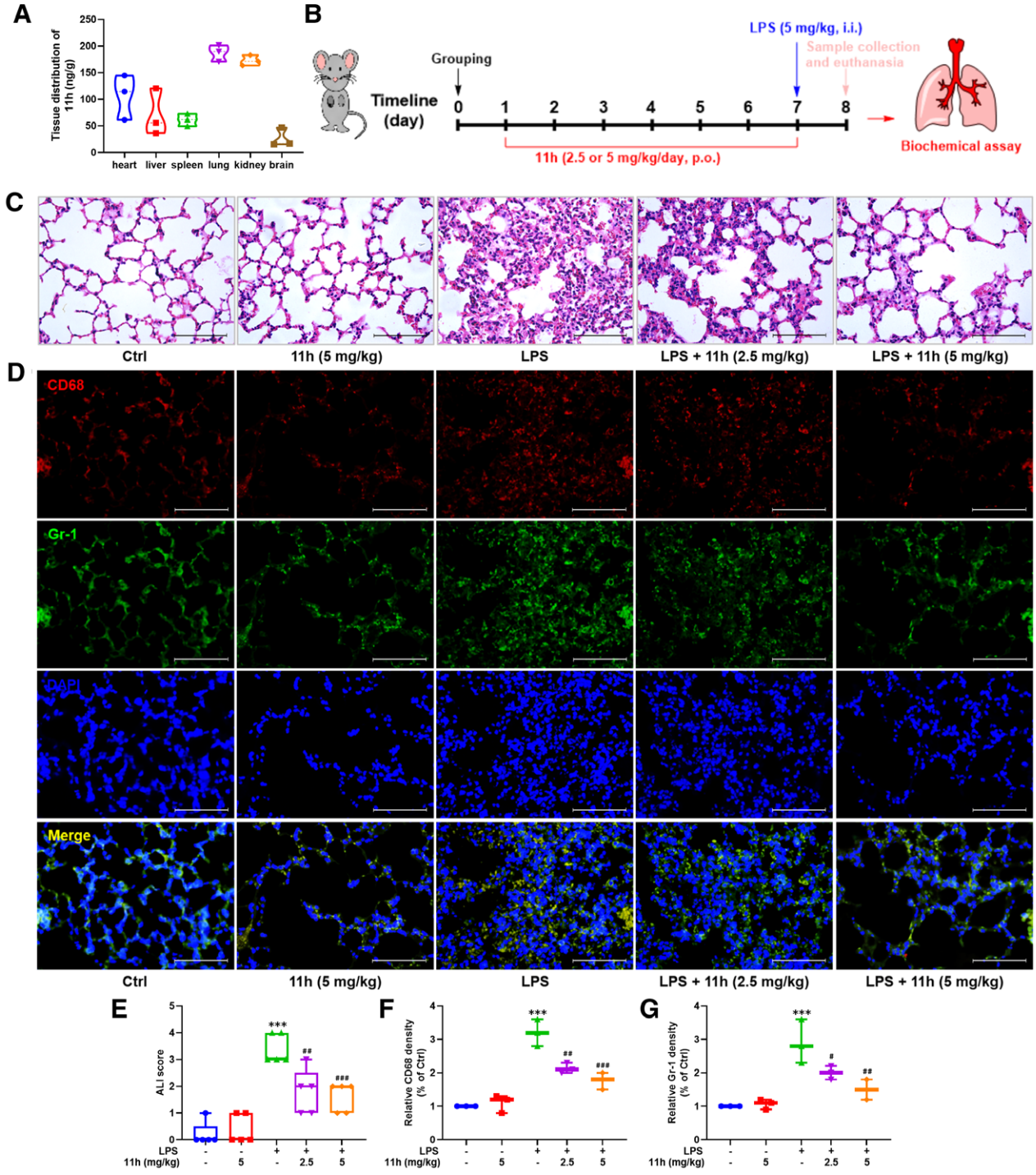

Figure 4. (A) Distribution of compound **11h** in different tissues. (B) The flow diagram of compound **11h** in the treatment of LPS-induced ALI. (C) Representative H&E plot. (D) Representative CD68 and Gr-1 staining plot. (E) ALI score. (F) Quantitative data of CD68 staining. (G) Quantitative data of Gr-1 staining, ***$P < 0.001$ *vs.* the control group, #$P < 0.05$, ##$P < 0.01$, ###$P < 0.001$ *vs.* the LPS group. ALI: Acute lung injury; LPS: Lipopolysaccharide.

protein COX-2 (Figure 7B and C). These results demonstrated the anti-inflammatory effect of compound **11h** against LPS-mediated ALI.

Inhibition of sEH by compound 11h attenuated oxidative stress through the Nrf2 pathway

In the course of ALI, the release of inflammatory cytokines promoted reactive oxygen species (ROS) production to break the redox system[28–29]. Collectively, LPS challenge led to the malondialdehyde (MDA) increase and the superoxide dismutase (SOD) and glutathione (GSH) decrease in ALI mice, whereas compound **11h** reversed these changes (Figure 8A). Accumulating studies previously have reported that sEH inhibition by TPPU, wedelolactone, or alisol B restores the redox balance *via* activating the classic signaling pathway—nuclear factor erythroid-2-related factor 2 (Nrf2) in the animal model of AD, ALI, and acute kidney injury[14–16,18,40–41]. As illustrated in Figures 8B and 9, compound **11h** activated the

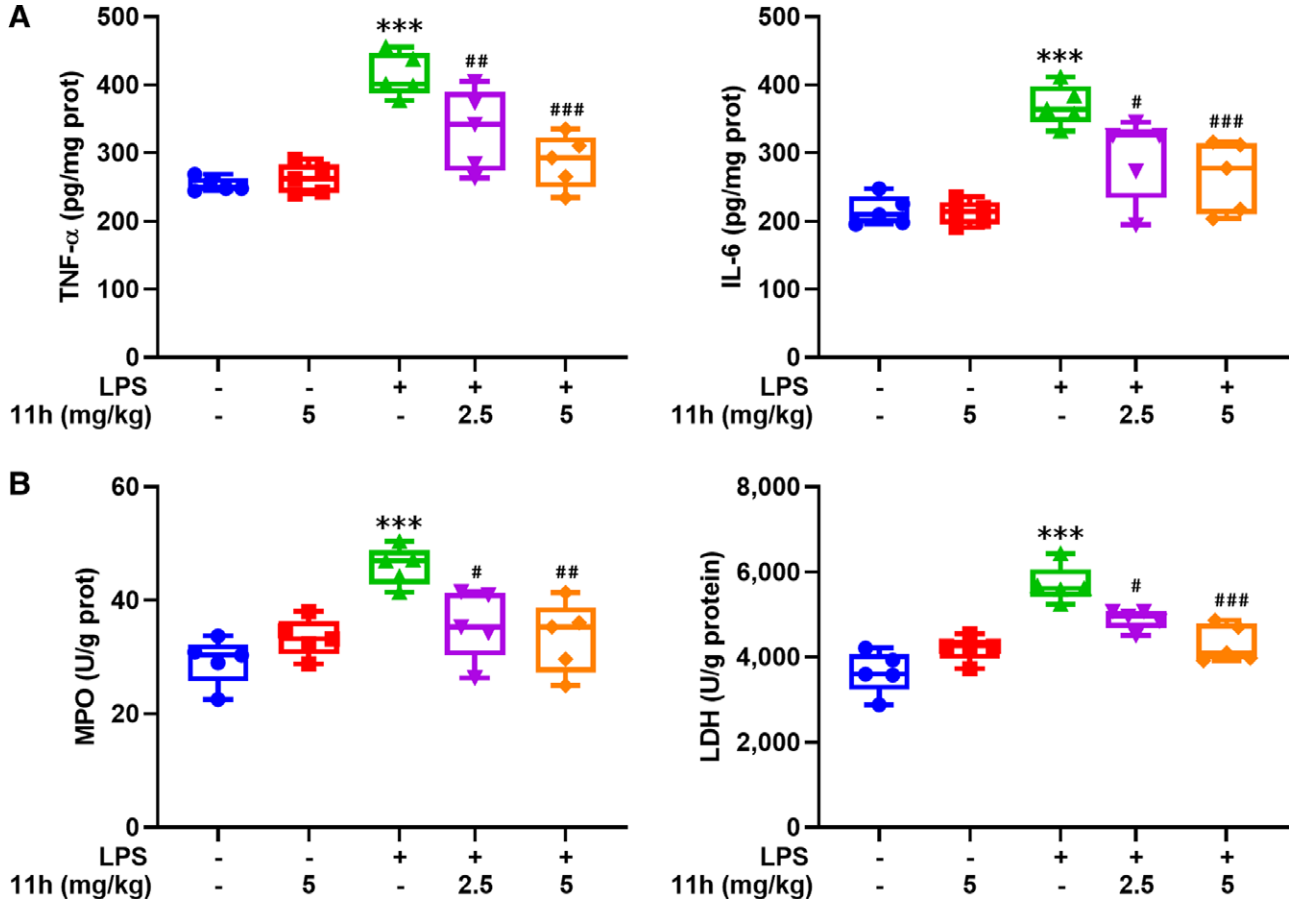

Figure 5. (A) Effects of compound **11h** toward TNF-α and IL-6. (B) Effects of compound **11h** toward MPO and LDH; ***$P < 0.001$ *vs.* the control group, #$P < 0.05$, ##$P < 0.01$, ###$P < 0.001$ *vs.* the LPS group. IL-6: Interleukin-6; LDH: Lactate dehydrogenase; LPS: Lipopolysaccharide; MPO: Myeloperoxidase; TNF-α: Tumor necrosis factor alpha.

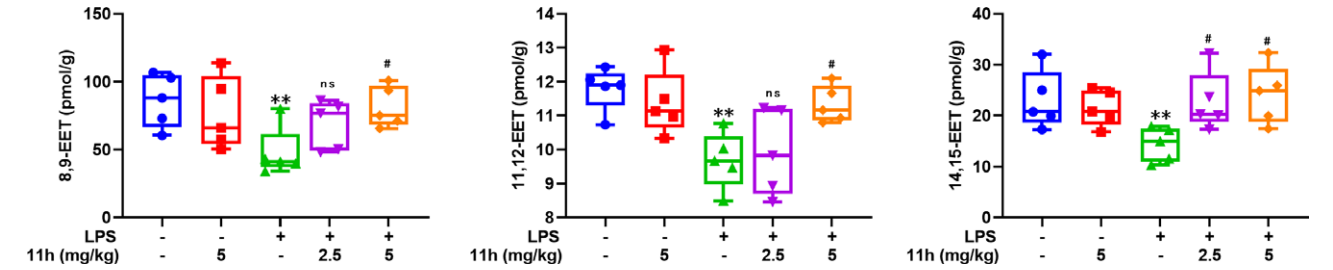

Figure 6. Effects of compound **11h** toward EETs, **$P < 0.01$ *vs.* the control group, #$P < 0.05$ *vs.* the LPS group. EETs: Epoxyeicosatrienoic acids; LPS: Lipopolysaccharide; ns: No significance.

Nrf2 pathway through the upregulation of its downstream proteins NAD(P)H: quinoneoxidoreductase-1 (NQO-1), glutamate-cysteine ligase catalytic subunit (GCLC), heme oxygenase-1 (HO-1), and glutamate-cysteine ligase modifier subunit (GCLM) (Figure 9A and B), and genes catalase (*CAT*) and *SOD1*, and downregulation of genes NADPH oxidase 2 and 4 (*NOX2* and *NOX4*) in LPS-mediated ALI mice (Figure 8B). These results suggested the effect of compound **11h** on the redox system *via* activating the Nrf2 pathway in ALI.

Conclusions

A library of urea-type derivatives was synthesized according to the skeleton of piperine. Among them, compounds **11e**, **11h**, **11j**, and **11o** showed potent inhibitory potentials toward sEH (IC_{50} values from 20 to 70 nM). Compound **11h** attenuated the ALI pathological course and LPS-mediated inflammation and redox unbalance through NF-κB and Nrf2 pathways *via* enhancing levels of EETs in LPS-exposed ALI mice after **11h** treatment. Molecular docking demonstrated that the aromatic unsaturated group of **11h** occupied a hydrophobic pocket and its urea group formed three hydrogen bonds with Asp333, Tyr381, and Tyr465, which stabilized the active conformation of the ligand. These findings demonstrated that compound **11h** served as a lead compound for developing sEH inhibitors and treating inflammatory diseases, such as ALI.

Conflict of interest statement

The authors declare no conflict of interest.

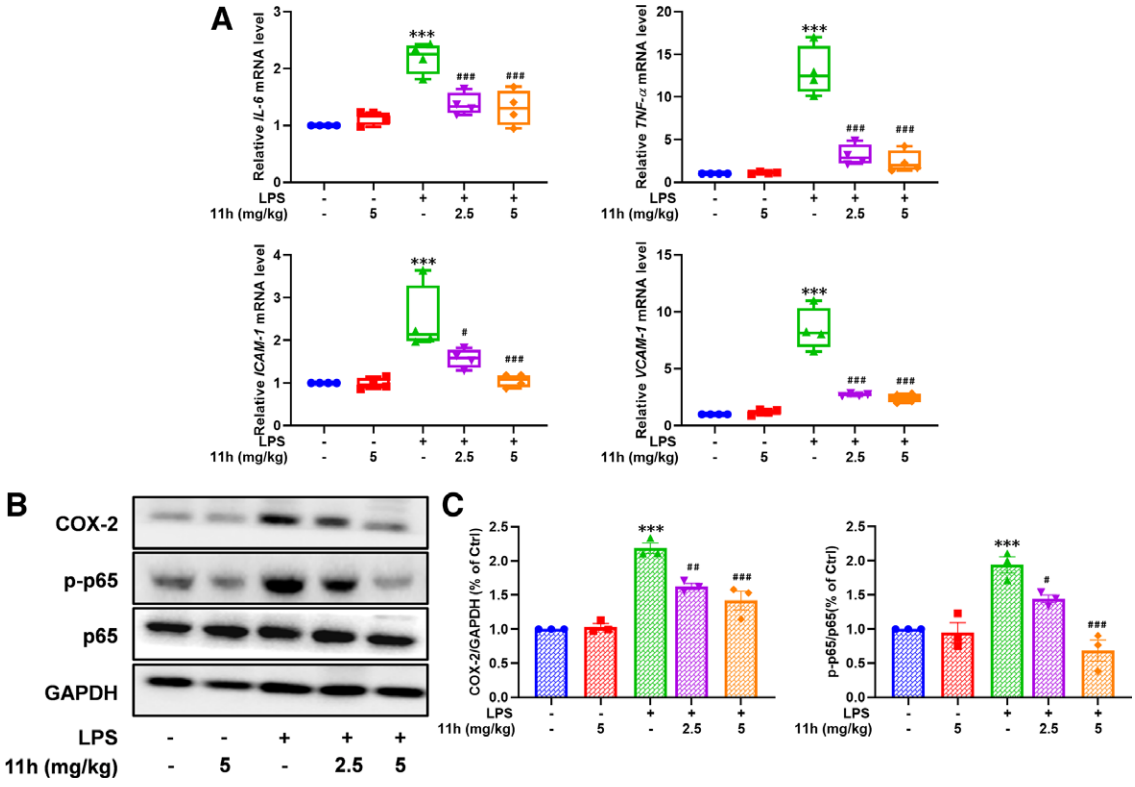

Figure 7. (A) Effects of compound **11h** toward mRNA expressions of *IL-6*, *TNF-α*, *ICAM-1*, and *VCAM-1*; (B) effects of compound **11h** toward the NF-κB pathway; (C) quantitative analysis for the protein levels in (B); ***$P < 0.001$ *vs.* the control group, #$P < 0.05$, ##$P < 0.01$, ###$P < 0.001$ *vs.* the LPS group. COX: Cyclooxygenase; *ICAM-1*: Intercellular cell adhesion molecule-1; *IL-6:* Interleukin-6; LPS: Lipopolysaccharide; NF-κB: Nuclear factor kappa B; TNF-α: Tumor necrosis factor alpha; *VCAM-1*: Vascular cell adhesion molecule-1.

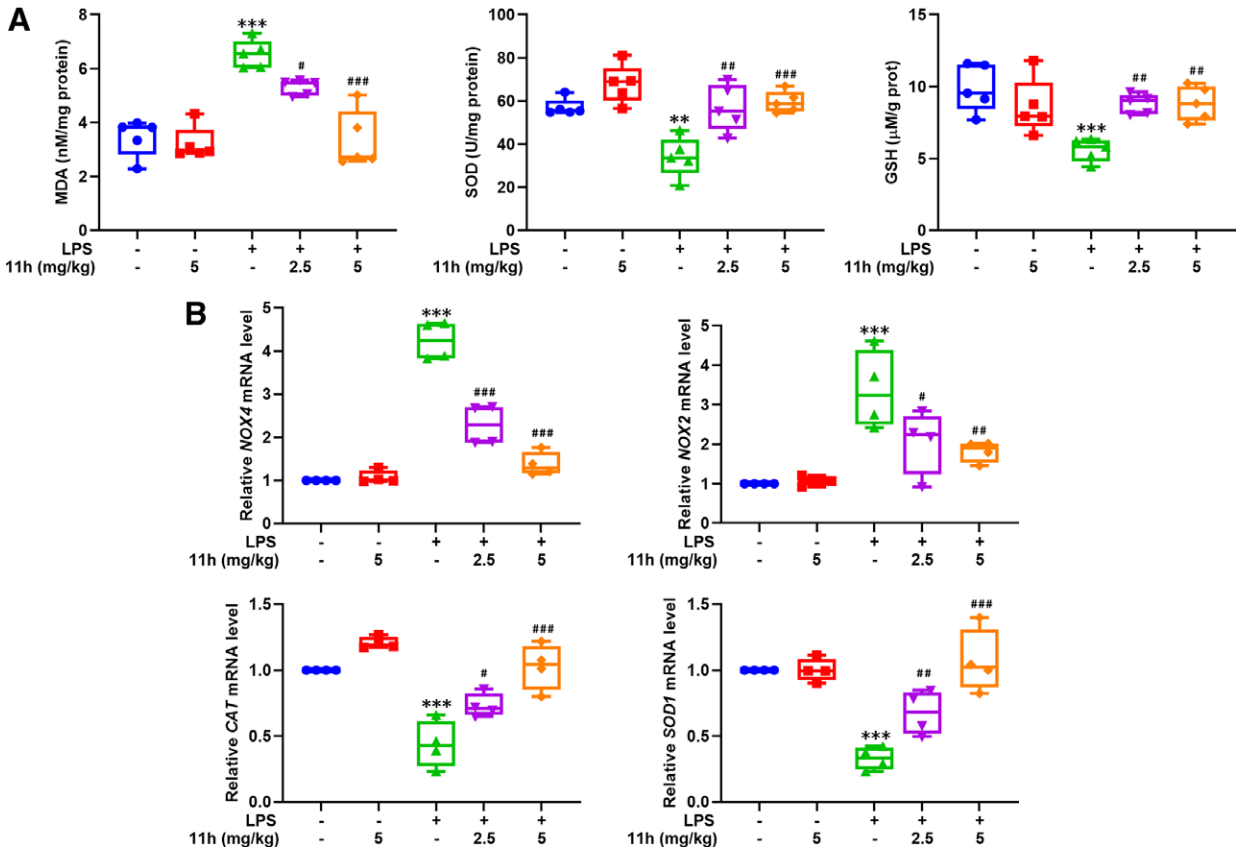

Figure 8. (A) Effects of compound **11h** toward MDA, SOD, and GSH. (B) Effects of compound **11h** toward mRNA expressions of *NOX2*, *NOX4*, *CAT*, and *SOD1*; **$P < 0.01$, ***$P < 0.001$ *vs.* the control group, #$P < 0.05$, ##$P < 0.01$, ###$P < 0.001$ *vs.* the LPS group. GSH: Glutathione; LPS: Lipopolysaccharide; MDA: Malondialdehyde; SOD: Superoxide dismutase.

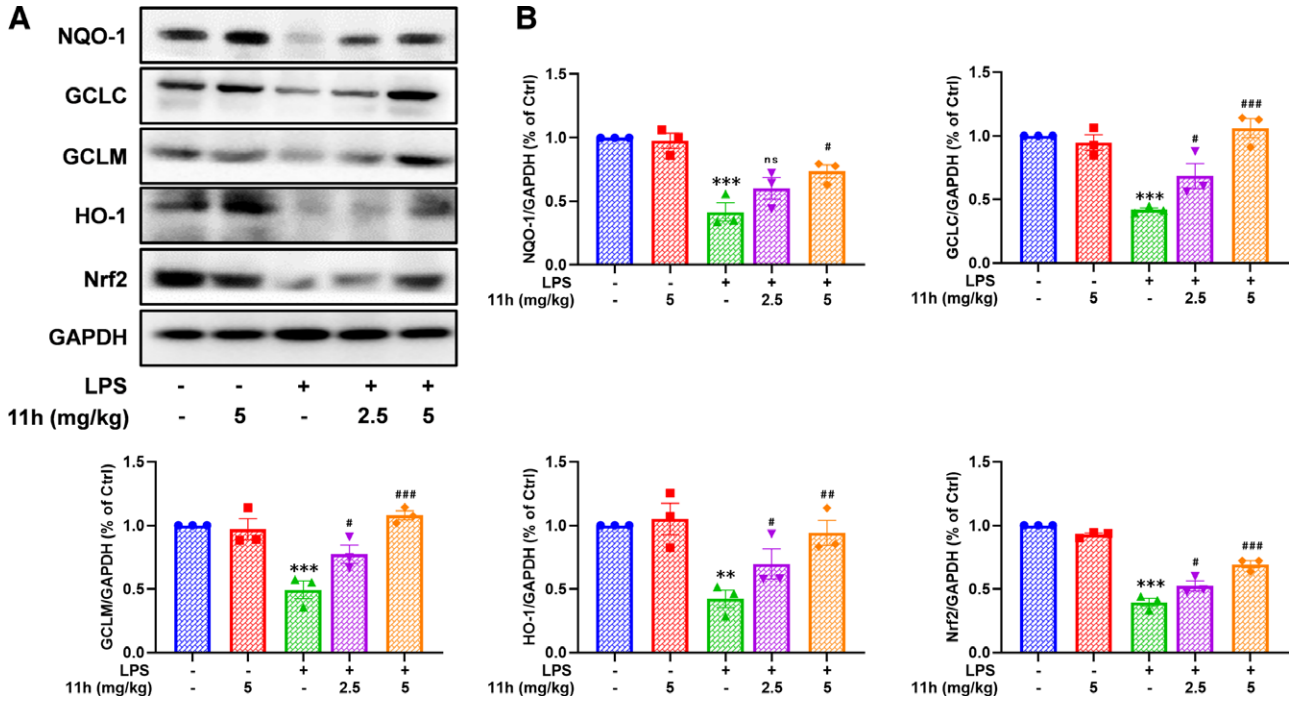

Figure 9. (A) Effects of compound **11h** toward the Nrf2 pathway. (B) Quantitative analysis for the protein levels in (A); $^{**}P < 0.01$, $^{***}P < 0.001$ *vs*. the control group, $\#P < 0.05$, $\#\#P < 0.01$, $\#\#\#P < 0.001$ *vs*. the LPS group. GAPDH: Glyceraldehyde-3-phosphate dehydrogenase; GCLC: Glutamate-cysteine ligase catalytic subunit; GCLM: Glutamate-cysteine ligase modifier subunit; HO-1: Heme oxygenase-1; LPS: Lipopolysaccharide; NQO-1: NAD(P)H: quinoneoxidoreductase-1; Nrf2: Nuclear factor erythroid-2-related factor 2; ns: No significance.

Funding

This work was supported by the National Natural Science Foundation of China (82274069 and 82003580), Shenzhen science and technology research and development funds (JCYJ20190808171803553 and 2022071718149001), Young Scientific and Technological Talents (Level Two) in Tianjin (QN20230212), Tianjin Education Commission Research Program Project (2024KJ004), Young Elite Scientists Sponsorship Program by China Association of Chinese Medicine (2022-QNRC2-B09), "1 + X" Research Project of the Second Hospital of Dalian Medical University (2024JJ11PT005), and Eaglet Plan Project of Tianjin University of Traditional Chinese Medicine (XJS2024101).

Author contributions

Da-Hong Yao, Xiao-Chi Ma, Bruce D. Hammock, and Cheng-Peng Sun designed the research. Juan Zhang and Xue-Tao Yang performed experiments, analyzed data, wrote, and revised the manuscript. Min Zhang and Qi-Meng Zhu analyzed the data. All authors read and approved the manuscript.

Ethical approval of studies and informed consent

Not applicable.

Acknowledgments

None.

Data availability

All relevant data are within the manuscript.

References

[1] Hanna VS, Hafez EAA. Synopsis of arachidonic acid metabolism: a review. *J Adv Res* 2018;11:23–32.
[2] Weller PF. Leukocyte lipid bodies—structure and function as "eicosasomes." *Trans Am Clin Climatol Assoc* 2016;127:328–340.
[3] Kano M, Ohno-Shosaku T, Hashimotodani Y, et al. Endocannabinoid-mediated control of synaptic transmission. *Physiol Rev* 2009;89(1):309–380.
[4] Dennis EA, Cao J, Hsu YH, et al. Phospholipase A2 enzymes: physical structure, biological function, disease implication, chemical inhibition, and therapeutic intervention. *Chem Rev* 2011;111(10):6130–6185.
[5] Bruntz RC, Lindsley CW, Brown HA. Phospholipase D signaling pathways and phosphatidic acid as therapeutic targets in cancer. *Pharmacol Rev* 2014;66(4):1033–1079.
[6] Sun CP, Zhang XY, Morisseau C, et al. Discovery of soluble epoxide hydrolase inhibitors from chemical synthesis and natural products. *J Med Chem* 2021;64(1):184–215.
[7] Newman JW, Morisseau C, Hammock BD. Epoxide hydrolases: their roles and interactions with lipid metabolism. *Prog Lipid Res* 2005;44(1):1–51.
[8] Neckar J, Kopkan L, Huskova Z, et al. Inhibition of soluble epoxide hydrolase by cis-4-[4-(3-adamantan-1-ylureido) cyclohexyl-oxy]benzoic acid exhibits antihypertensive and cardioprotective actions in transgenic rats with angiotensin II-dependent hypertension. *Clin Sci (Lond)* 2012;122(11):513–525.
[9] Imig JD, Zhao X, Capdevila JH, et al. Soluble epoxide hydrolase inhibition lowers arterial blood pressure in angiotensin II hypertension. *Hypertension* 2002;39(2 Pt 2):690–694.
[10] Bergmann CB, McReynolds CB, Wan D, et al. sEH-derived metabolites of linoleic acid drive pathologic inflammation while impairing key innate immune cell function in burn injury. *Proc Natl Acad Sci U S A* 2022;119(13):e2120691119.
[11] Deng J, Yang H, Haak VM, et al. Eicosanoid regulation of debris-stimulated metastasis. *Proc Natl Acad Sci U S A* 2021;118(41):e2107771118.
[12] Hevler JF, Zenezeni Chiozzi R, Cabrera-Orefice A, et al. Molecular characterization of a complex of apoptosis-inducing factor 1 with cytochrome c oxidase of the mitochondrial respiratory chain. *Proc Natl Acad Sci U S A* 2021;118(39):e2106950118.
[13] Qin JJ, Jin HZ, Zhu JX, et al. New sesquiterpenes from Inula japonica Thunb. with their inhibitory activities against

LPS-induced NO production in RAW264.7 macrophages. *Tetrahedron* 2010;66(1):9379–9388.
[14] Sun CP, Zhang XY, Zhou JJ, et al. Inhibition of sEH via stabilizing the level of EETs alleviated Alzheimer's disease through GSK3beta signaling pathway. *Food Chem Toxicol* 2021;156:112516.
[15] Sun CP, Zhou JJ, Yu ZL, et al. Kurarinone alleviated Parkinson's disease via stabilization of epoxyeicosatrienoic acids in animal model. *Proc Natl Acad Sci U S A* 2022;119(9):e2118818119.
[16] Zhang J, Zhang M, Huo XK, et al. Macrophage inactivation by small molecule wedelolactone via targeting sEH for the treatment of LPS-induced acute lung injury. *ACS Cent Sci* 2023;9(3):440–456.
[17] Zhang J, Yang FY, Zhu QM, et al. Inhibition effect of 1-acetoxy-6alpha-(2-methylbutyryl)eriolanolide toward soluble epoxide hydrolase: multispectral analysis, molecular dynamics simulation, biochemical, and in vitro cell-based studies. *Int J Biol Macromol* 2023;235:123911.
[18] Zhang J, Luan ZL, Huo XK, et al. Direct targeting of sEH with alisol B alleviated the apoptosis, inflammation, and oxidative stress in cisplatin-induced acute kidney injury. *Int J Biol Sci* 2023;19(1):294–310.
[19] Feng ZQ, Ding J, Zhu MZ, et al. Discovery of a novel lead characterized by a stilbene-extended scaffold against sepsis as soluble epoxide hydrolase inhibitors. *Eur J Med Chem* 2024;266:116113.
[20] Khan MAH, Nolan B, Stavniichuk A, et al. Dual soluble epoxide hydrolase inhibitor—farnesoid X receptor agonist interventional treatment attenuates renal inflammation and fibrosis. *Front Immunol* 2023;14:1269261.
[21] Burmistrov VV, Morisseau C, Danilov DV, et al. Fluorine and chlorine substituted adamantyl-urea as molecular tools for inhibition of human soluble epoxide hydrolase with picomolar efficacy. *J Enzyme Inhib Med Chem* 2023;38(1):2274797.
[22] Kong L, Li J, Bai Y, et al. Inhibition of soluble epoxide hydrolase enhances the dentin-pulp complex regeneration mediated by crosstalk between vascular endothelial cells and dental pulp stem cells. *J Transl Med* 2024;22(1):61.
[23] Chen Y, Chen L, Xu H, et al. Structure-directed discovery of potent soluble epoxide hydrolase inhibitors for the treatment of inflammatory diseases. *J Med Chem* 2023;66(4):2979–3009.
[24] Chen D, Whitcomb R, MacIntyre E, et al. Pharmacokinetics and pharmacodynamics of AR9281, an inhibitor of soluble epoxide hydrolase, in single- and multiple-dose studies in healthy human subjects. *J Clin Pharmacol* 2012;52(3):319–328.
[25] Hammock BD, McReynolds CB, Wagner K, et al. Movement to the clinic of soluble epoxide hydrolase inhibitor EC5026 as an analgesic for neuropathic pain and for use as a nonaddictive opioid alternative. *J Med Chem* 2021;64(4):1856–1872.
[26] Zhao WY, Yan JJ, Zhang M, et al. Natural soluble epoxide hydrolase inhibitors from Inula britanica and their potential interactions with soluble epoxide hydrolase: insight from inhibition kinetics and molecular dynamics. *Chem Biol Interact* 2021;345:109571.
[27] Gomez GA, Morisseau C, Hammock BD, et al. Human soluble epoxide hydrolase: structural basis of inhibition by 4-(3-cyclohex ylureido)-carboxylic acids. *Protein Sci* 2006;15(1):58–64.
[28] Zhang J, Zhang M, Zhang WH, et al. Total flavonoids of Inula japonica alleviated the inflammatory response and oxidative stress in LPS-induced acute lung injury via inhibiting the sEH activity: insights from lipid metabolomics. *Phytomedicine* 2022;107:154380.
[29] Zhang J, Zhang M, Zhang WH, et al. Total terpenoids of Inula japonica activated the Nrf2 receptor to alleviate the inflammation and oxidative stress in LPS-induced acute lung injury. *Phytomedicine* 2022;107:154377.
[30] Zhang M, Zhang J, Wang C, et al. Biotransformation of 18beta-glycyrrhetinic acid by human intestinal fungus Aspergillus niger RG13B1 and the potential anti-inflammatory mechanism of its metabolites. *J Agric Food Chem* 2022;70(48):15104–15115.
[31] Zhang J, Yan JK, Dong HJ, et al. Dimeric sesquiterpenoids with anti-inflammatory activities from Inula britannica. *Chin J Nat Med* 2024;22:1–13.
[32] Dong L, Zhou Y, Zhu ZQ, et al. Soluble epoxide hydrolase inhibitor suppresses the expression of triggering receptor expressed on myeloid cells-1 by inhibiting NF-kB activation in murine macrophage. *Inflammation* 2017;40(1):13–20.
[33] Zhou Y, Liu T, Duan JX, et al. Soluble epoxide hydrolase inhibitor attenuates lipopolysaccharide-induced acute lung injury and improves survival in mice. *Shock* 2017;47(5):638–645.
[34] Luo XQ, Duan JX, Yang HH, et al. Epoxyeicosatrienoic acids inhibit the activation of NLRP3 inflammasome in murine macrophages. *J Cell Physiol* 2020;235(12):9910–9921.
[35] Lan XF, He QY, Shi YM, et al. Herbal medicine in the treatment of COVID-19 based on the gut–lung axis. *Acupunct Herb Med* 2022;2:172–183.
[36] Feng YL, Xu XR, Zhu QM, et al. Aucklandiae radix targeted PKM2 to alleviate ulcerative colitis: insights from the photocrosslinking target fishing technique. *Phytomedicine* 2024;134:155973.
[37] Zhang J, Zhang R, Li W, et al. IkappaB kinase beta (IKKbeta): structure, transduction mechanism, biological function, and discovery of its inhibitors. *Int J Biol Sci* 2023;19(13):4181–4203.
[38] Nie Y, Huang MY, Yang TY, et al. Ferulic acid reduces inflammatory response induced by radiation through Sirt1-NLRP3 pathway. *Acupunct Herb Med* 2024;4(3):367–374.
[39] Shao Y, Su R, Wang Y, et al. Drug co-administration in the tumor immune microenvironment of hepatocellular carcinoma. *Acupunct Herb Med* 2023;3(3):189–199.
[40] Zhang J, Zhang M, Zhu QM, et al. Allosteric regulation of Keap1 by 8β-hydroxy-α-cyclocostunolide for the treatment of acute lung injury. *Acta Pharm Sin B* 2024;14:4174–4178.
[41] Wang W, Xiong LL, Wu YL, et al. New lathyrane diterpenoid hybrids have anti-inflammatory activity through the NF-κB signaling pathway and autophagy. *Acta Mater Med* 2022;1:224–243.